LETTER • **OPEN ACCESS**

Quantitative measurements of singlet molecular oxygen in a low pressure ICP

To cite this article: Samuel D A Rogers *et al* 2021 *Plasma Sources Sci. Technol.* **30** 09LT02

OPEN ACCESS
IOP Publishing

Letters
Plasma Sources Science and Technology

Plasma Sources Sci. Technol. **30** (2021) 09LT02 (8pp)
https://doi.org/10.1088/1361-6595/ac2044

Letter

Quantitative measurements of singlet molecular oxygen in a low pressure ICP

Samuel D A Rogers[1], Amelia Bond[1], Robert Peverall[1], Gus Hancock[1], Colin M Western[2] and Grant A D Ritchie[1,*]

[1] Department of Chemistry, Physical and Theoretical Chemistry Laboratory, The University of Oxford, South Parks Road, Oxford OX1 3QZ, United Kingdom
[2] School of Chemistry, University of Bristol, Cantock's Close, Bristol, BS8 1TS, United Kingdom

E-mail: grant.ritchie@chem.ox.ac.uk

Received 15 July 2021, revised 11 August 2021
Accepted for publication 23 August 2021
Published 27 September 2021

Abstract

We present measurements of the densities and temperatures (rotational and translational) of the metastable $a^1\Delta_g$ ($v = 0$) state of O_2 in a cylindrically symmetric RF driven plasma operating in inductive mode at 100 mTorr total pressure and 300 W applied power. Line-of-sight absorption across the plasma region was determined by diode laser cavity ringdown spectroscopy on the (0, 0) vibrational band of the $O_2(b^1\Sigma_g^+) \leftarrow O_2(a^1\Delta_g)$ transition near 1.9 μm. Four rotational quantum states were studied, with a population distribution corresponding to a rotational temperature of 346 ± 38 K. The translational temperature was determined to be 359 ± 16 K from the width of the strongest absorption line, $Q(12)$, and in equilibrium with the rotational distribution. The absolute concentration of $O_2(a^1\Delta_g, v = 0)$ was measured as $(9.5 \pm 1.3) \times 10^{13}$ cm^{-3}, and corresponds to an apparent (3.5 ± 0.45)% contribution to the total number density. Time-resolved CRDS measurements following plasma extinction were used to deduce a wall loss coefficient, γ, of $(2.8 \pm 0.3) \times 10^{-3}$ on predominantly Al surfaces. Surmising reasonable concentrations for $O_2(b^1\Sigma_g^+)$ and an upper limit for the vibrational temperature places the total contribution of $O_2(a^1\Delta_g)$ at between 3.6% and 5.85%. The variation of the $O_2(a^1\Delta_g, v = 0)$ state concentration with RF power shows a clear transition from the E to H mode excitation near an applied power of 150 W. Allan variance analysis yields a minimum measurable concentration of $O_2(a^1\Delta_g, v = 0)$ of 1.1×10^{12} cm^{-3} over 100 ringdown events, an order of magnitude more sensitive than previously reported.

Keywords: metastable oxygen, cavity ringdown spectroscopy, inductively coupled plasma, $O_2(a^1\Delta_g)$, singlet oxygen, surface loss

(Some figures may appear in colour only in the online journal)

* Author to whom any correspondence should be addressed.

1. Introduction

Oxygen containing discharges are ubiquitous in industry providing the means for cleaning, oxidising, etching and deposition [1–4], and hence extensive efforts have been made to model these systems [5–11]. Understandably, modelling predictions have outpaced experimental capabilities, and nowhere is this more evident than for pure oxygen plasmas which contain numerous species known to be important but which are inherently difficult to measure. Perhaps the exemplar of this is the first excited state of molecular oxygen, so-called singlet oxygen, $O_2(a^1\Delta_g)$. The $a^1\Delta_g$ state lies about 1 eV above the ground state and is metastable with regard to radiative decay (radiative lifetime = 72 min [12]) and is relatively stable against collisional quenching as a consequence of the doubly forbidden nature of the $O_2(a^1\Delta_g) \rightarrow O_2(X^3\Sigma_g^-)$ transition [13–15]. Generally, models predict $O_2(a^1\Delta_g)$ concentrations of ~10% of the total gas phase number density and implicate this species in enhanced dissociation, attachment and ionisation processes [5, 7]. Despite its clear importance, it is difficult to measure quantitatively under technologically relevant conditions with readily available light sources. Indeed, except the work by Wegner *et al* [16] who utilised dual wavelength VUV spectroscopy at ca 128.5 nm, there have been no absolute measurements of this species in a low pressure (<1 Torr) plasma reactor. Other studies that have been reported have generally been from discharge tube arrangements at pressures >1 Torr and in gas mixtures [17–20]. In this letter we report measurements of $O_2(a^1\Delta_g)$ using diode laser cavity ringdown spectroscopy (CRDS), recording absorption profiles under industrially important conditions in an inductively coupled rf (13.56 MHz) plasma reactor operating with 100 mTorr of pure O_2 (99.999% BOC) and as a function of power up to 300 W. These conditions are within the typical parameter space of oxygen plasma models [6–8, 11].

The experimental arrangement and the plasma chamber used in this study have been described in detail elsewhere [21] and so only a brief description is given here. The ICP chamber is of cylindrical geometry (height × width = 21 × 35 cm) and is powered through a quartz dielectric interface (diameter = 25 cm) via a coil-type rf electrode. Measurements are made approximately half way down the chamber through two opposing baffle arms (i.d. 9 mm, length 15 cm) at the end of which sit high reflectivity mirrors (R = 99.99%, Layertec GmbH) required for CRDS. The laser source is a fibre coupled distributed feedback diode laser (Eblana, power ~ 3 mW), operating at wavelengths around 1908 nm at room temperature and probing individual rotational lines within the $O_2(b^1\Sigma_g^+) \leftarrow O_2(a^1\Delta_g)$ (0, 0) band. The CRDS arrangement is similar to that presented in [22, 23], and uses an acousto-optic modulator to interrupt the probe laser, thus generating the requisite ringdown signals.

2. Results and discussion

Cavity ringdown spectra of four Q branch lines ($J'' = 4$, 6, 10 and 12) are shown in figure 1. The data are the averages of multiple individual CRD spectra for each line (between three and six depending on the signal-to-noise ratio) collected at a pressure of 100 mTorr. In each case τ was converted to an absorption coefficient, α (numerically equal to the absorption cross-section multiplied by the concentration), using the equation $(1/\tau) - (1/\tau_0) = \alpha c$, where τ and τ_0 are the ringdown times with and without absorber. Data are fitted with a Gaussian function (pressure broadening is negligible) to reveal the line-of-sight integrated-absorption coefficient (α_{int}) and average translational temperature, T_{tr}, (determined from the full-width half-maximum (FWHM) of the Gaussian function). For $Q(12)$, the transition with the highest signal to noise ratio, the width of the averaged spectrum corresponds to a value of T_{tr} of (359 ± 16) K. To confirm this, each of the four individual $Q(12)$ spectra were also fitted with Gaussian functions and the FWHM of each found. The average temperature from this was (370 ± 23) K, in good agreement with that from the averaged spectrum.

Absorption cross sections for the selected transitions were calculated using the Einstein A-factor for the band calculated by Gupta *et al* [19] of 1.26×10^{-3} s^{-1}, which is in good agreement with the experimental value of $(1.2 \pm 0.25) \times 10^{-3}$ s^{-1} [24]. The A-factor was first used to derive an effective vibronic transition moment using the standard equation (see, for example, equation (7) in Larsson [25]). Notably, this calculation quantifies the strength of the electric quadrupole transition in terms of an electric dipole moment equivalent value. This vibronic transition moment was then converted to a line strength for each rotational transition by multiplying by the rotational line intensity factor, $\mathcal{S}_{J'J''}$ (also known as the Hönl–London factor). Hönl–London factors are tabulated by Kovacs [26] and for this quadrupole allowed transition were originally derived by Chiu [27]. For a Q-branch line the Hönl–London factor is given by:

$$\mathcal{S}_{J'J''} = \frac{3(2J''+1)(J''+2)(J''-1)}{(2J''-1)(2J''+3)}. \qquad (1)$$

This value is a factor of 3/2 larger than that tabulated in Kovacs [26], and ensures that the sum rule for $\mathcal{S}_{J'J''}$ set out by Whiting *et al* [28] is respected (the sum of the values in Kovacs [26] for this transition is 4/3 $(2J'' + 1)$, see Whiting *et al* [29]). The values derived from this formula agree with those determined using PGOPHER [30, 31] provided that a scaling factor of 5/3 is applied to the values from PGOPHER as recommended for a quadrupolar transition [32]. The line strengths were then converted to rotational state specific integrated cross sections, $\sigma_{int,J''}$ using the standard equations [33]. We note that this method, using a dipole moment equivalent value, gives the same result as a more rigorous consideration of transition quadrupole moments. In the more rigorous treatment care must be taken to ensure the correct definition of the quadrupole moment operator is used so as to be compatible with the $\mathcal{S}_{J'J''}$ sum rule already mentioned. We will present this more rigorous approach in a future publication.

For a transition originating from an initial state J'', $\alpha_{int} = N_{av,J''}\sigma_{int,J''}$, where $N_{av,J''}$ is the line-of-sight average number density in the J'' rotational state. The calculated integrated cross sections, $\sigma_{int,J''}$, therefore enable line-of-sight averaged rotational state populations to be calculated from the

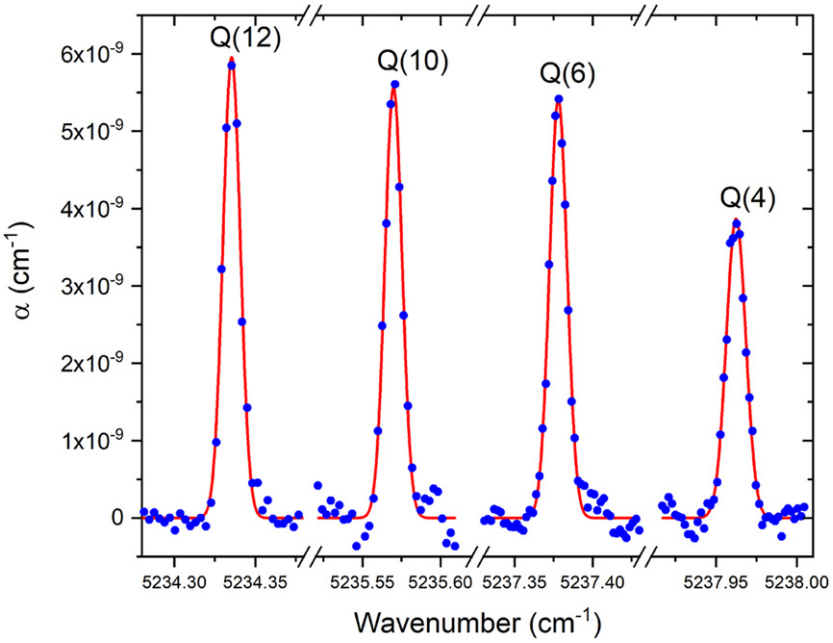

Figure 1. CRD spectra of $Q(12)$, $Q(10)$, $Q(6)$ and $Q(4)$ lines of the $O_2(b^1\Sigma_g^+) \leftarrow O_2(a^1\Delta_g)$ (0, 0) vibrational band recorded at 100 mTorr total pressure. The red line is the Gaussian fit to the data.

experimental data. For the $Q(12)$ transition at 5234.33 cm^{-1}, $\sigma_{int,J''} = 2.3 \times 10^{-23}$ cm^2 cm^{-1}.

In this chamber the mirrors are located at the ends of baffle arms which extend from the (reactive) plasma volume, and in order to deduce the average number density of a given rotational state in the plasma volume, $N_{J''}$, the line-of-sight average number density, $N_{av,J''}$, must be multiplied by the ratio $(L/l) = 77/(35 + 2h)$, where l and L are the actual absorption length (or the effective length over which the absorber exists) and the physical length of the cavity, respectively, and h is a (relatively small) pressure dependent $1/e$ scale length that represents the penetration of $O_2(a^1\Delta_g)$ into the baffle arms.

In the absence of discharge conditions, such as in the baffle arms, the $O_2(a^1\Delta_g)$ loss is dominated by surface deactivation. Thus, in order to quantify this wall loss the lifetime of $O_2(a^1\Delta_g)$ in the chamber was measured by modulating the plasma on and off at 0.5 Hz. The laser was set at the line centre for the $Q(12)$ transition and the ringdown time recorded for 2 h. The data were recorded in 3 ms windows corresponding to ca 40 ringdown events. The temporal decay in α (and hence $O_2(a^1\Delta_g)$ concentration) was fitted with an exponential decay as shown in figure 2 and yields lifetimes $(1/e)$ for $O_2(a^1\Delta_g)$ of (152 ± 17) ms at 100 mTorr and (128 ± 7) ms at 75 mTorr. Chantry [34] showed that, under conditions where species loss is dominated by diffusion and deactivation or reaction at the walls, the fundamental diffusion mode loss is well represented by a lifetime, τ_D, such that:

$$\tau_D = \frac{p\Lambda_0^2}{D} + \frac{2l_0(2-\gamma)}{v\gamma}, \tag{2}$$

where D is the diffusion coefficient, l_0 is the chamber's volume to surface area ratio (4.8 cm), v is the mean thermal speed of oxygen molecules and Λ_0 is the geometric diffusion length (4.9 cm) [22]. Using the Chantry formalism allows calculation of the surface loss probability, γ, for $O_2(a^1\Delta_g)$ at the two pressures studied. The diffusion coefficient is 3.05×10^4 cm^2 s^{-1} Pa (assumed to be the same as for $O_2(X^3\Sigma_g^-)$) [35], and the mean thermal speed of O_2 calculated as 4.81×10^2 m s^{-1} ($T \sim 350$ K). The measured lifetimes correspond to $\gamma = (2.8 \pm 0.3) \times 10^{-3}$ and $(3.3 \pm 0.2) \times 10^{-3}$ at 100 and 75 mTorr, respectively. These values are in good agreement with previous observations by Derzsi *et al* [36] who deduced a γ value of 6×10^{-3} in a chamber constructed from aluminium which had been exposed to a pure oxygen plasma at ~100 mTorr. Under such conditions aluminium surfaces exist with an oxidised layer, leading to the low wall loss coefficient we observe. This is in contrast to metals such as Ag, Pt and Ni where the lack of such an oxidised layer leads to a wall loss coefficient an order of magnitude higher [37].

Penetration into the steel baffle arms can be estimated by use of the Chantry formalism and Fick's second law. For the cylindrical steel arms ${\Lambda_0}^{arms} = 0.62$ cm and ${l_0}^{arms} = 0.74$ cm and $\gamma = 7 \times 10^{-3}$ (a value measured for iron [37] but regularly used for steel) yielding a lifetime in the arms of 9×10^{-3} s (and a loss rate $k = 1/\tau_D = 112$ s^{-1}). Fick's second law, including a loss term, may be written as:

$$\frac{dN(x)}{dt} = \frac{D}{p}\frac{d^2N(x)}{dx^2} - kN(x) = 0. \tag{3}$$

At equilibrium the number density, $N(x)$, is invariant with time, hence equation (3) may be set to zero. Under these conditions equation (3) has the following solution:

$$N(x) = N(x=0)\exp\left(-\sqrt{\frac{kp}{D}}x\right), \tag{4}$$

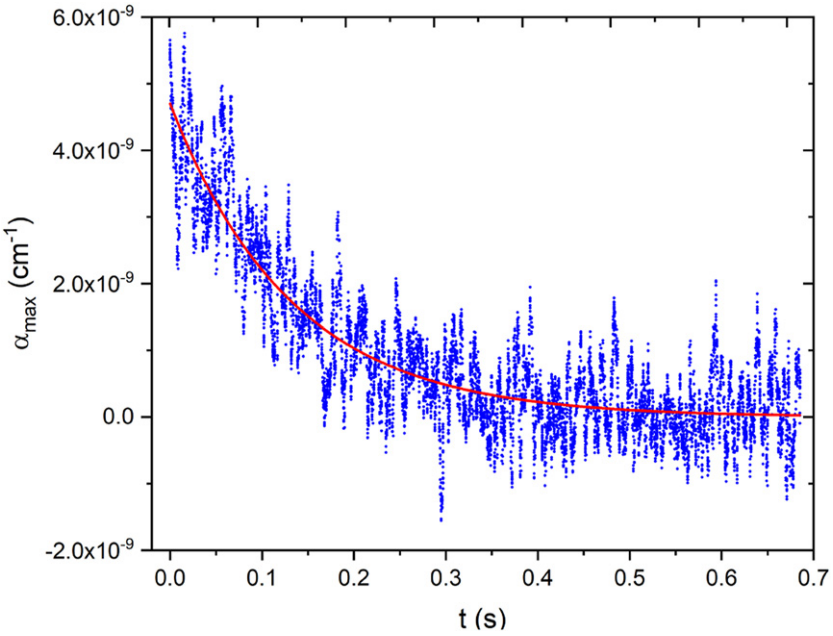

Figure 2. Graph showing the change in maximum absorption coefficient for the $Q(12)$ line after the plasma is extinguished. The lifetime $(1/e)$ for the first order decay of $O_2(a^1\Delta_g, v = 0)$ is (152 ± 17) ms.

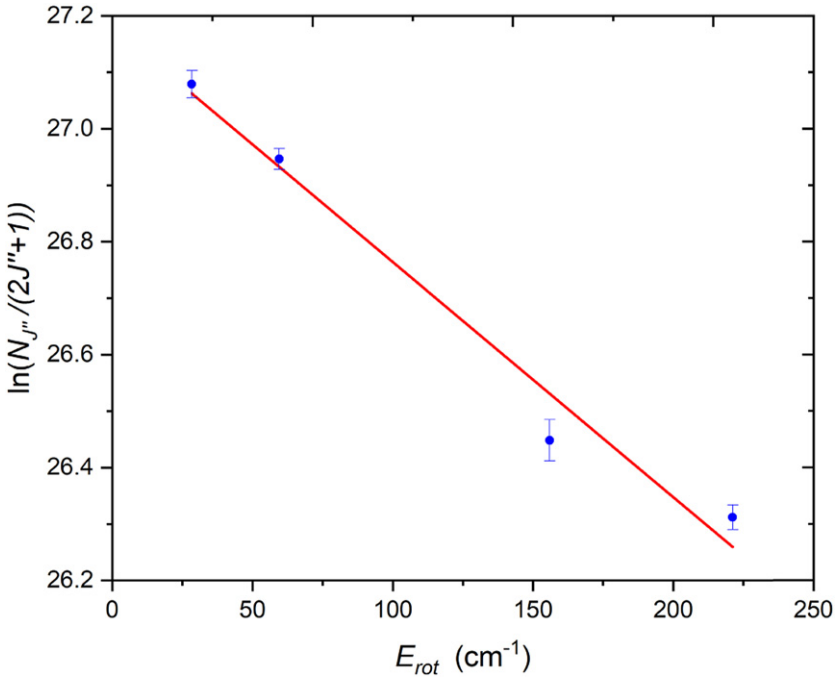

Figure 3. Boltzmann plot to determine $T_{\rm rot}$ and $N_{v=0}$ for $O_2(a^1\Delta_g)$ at 100 mTorr.

where $N(x = 0)$ is the density in the plasma chamber and $N(x)$ is the density in the baffle arm a distance, x, from the chamber. This function has a $1/e$ scale length, $h = (D/kp)^{1/2}$ which is ~5 cm at 100 mTorr and corresponds to an absorption length adjustment of (77/45).

The number density in each rotational level, $N_{J''}$, can then be used to find the number density in the lowest vibrational level, $N_{v=0}$, if the rotational partition function, $q_{\rm rot}$, is known. A key element in this calculation is the rotational temperature, $T_{\rm rot}$, which can be determined from a Boltzmann plot according to:

$$\frac{N_{J''}}{N_{v=0}} = \frac{(2J'' + 1)\exp\left(\frac{-E_{\rm rot}}{k_{\rm B}T_{\rm rot}}\right)}{q_{\rm rot}}. \tag{5}$$

Figure 3 shows such a plot for the rotationally resolved number densities determined from the data in figure 1.

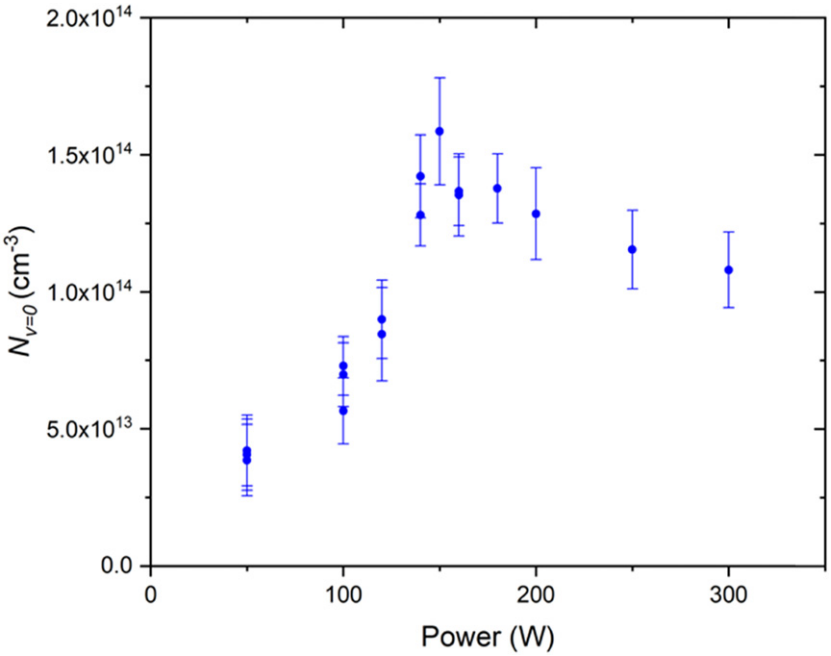

Figure 4. The measured $O_2(a^1\Delta_g, v = 0)$ number density as a function of power at 100 mTorr pressure, clearly illustrating the E/H switch-over region. Densities are corrected for estimated $O_2(b^1\Sigma_g^+, v = 0)$ populations, see text.

Taking the molecular constants for $O_2(a^1\Delta_g)$ from the work of Drouin *et al* [38] the gradient of this plot yields $T_{rot} = (346 \pm 38)$ K. This is in good agreement with the translational temperature determined from the FWHM of the individual spectral lines. The intercept in figure 3, along with this temperature, gives $N_{v=0} = (9.5 \pm 1.3) \times 10^{13}$ cm^{-3}. Thus, at a total pressure of 100 mTorr, the *apparent* proportion of the sample that is $O_2(a^1\Delta_g, v = 0)$ is (3.5 ± 0.45)%. We note that, formally, the absorption measurements yield the *difference* in population between the lower and upper states of the probed transitions. Usually the upper state population can be neglected as it is much smaller, but that is not necessarily the case here. The $b^1\Sigma_g^+$ state of molecular oxygen is also metastable and has been predicted to have significant concentrations under certain circumstances [11, 39]. However, equilibrium considerations based on the relative electron impact production and loss rates of the $a^1\Delta_g$ and $b^1\Sigma_g^+$ states, which includes contributions from the $O(^3P)$ chemistry [22, 40], indicate that the $b^1\Sigma_g^+$ state has a maximum concentration *ca* 15% of that of the $a^1\Delta_g$ state for the wall loss rates recorded here. We note that additional fast loss processes for the $b^1\Sigma_g^+$ state, namely loss at the wall with γ potentially as high as 0.1 [11] and energy transfer reactions with $O(^3P)$ [40] make it likely that the actual density of $O_2(b^1\Sigma_g^+)$ is significantly below our upper bound estimate of 15%. These considerations yield a corrected $a^1\Delta_g$ contribution of (4.1 ± 0.5)%. Taking account of a probable upper limit to the vibrational temperature of ~1300 K (low v) and non-thermal distribution (high v) [41], which has been reported recently for slightly different conditions (500 W, 80 mTorr) increases the total $O_2(a^1\Delta_g)$ contribution by 25% to (5.15 ± 0.7)%. Thus, with reasonable confidence we estimate that the total contribution of $O_2(a^1\Delta_g)$ lies between the bounds of 3.6%–5.85%, corresponding to a concentration of between 1×10^{14} cm^{-3} and 1.63×10^{14} cm^{-3}.

Further $Q(12)$ spectra were gathered at plasma powers between 50 and 300 W to study how the $O_2(a^1\Delta_g)$ density varies across the E/H (capacitive/inductive) switchover region. This is important because, as well as providing information about the fundamental processes occurring in the plasma, knowledge of the varying densities of these reactive species allows for optimal process efficiency in industrial applications. Across the power range we observe a linear increase in the translational temperature from *ca* 310 K (50 W) to 360 K (300 W). By assuming that T_{tr} is equilibrated with T_{rot} we infer a total number density, $N_{v=0}$, in the ground vibrational level as shown in figure 4.

Figure 4 illustrates that the E/H switchover occurs between 130 and 150 W. The trend in number density as a function of power can be qualitatively explained by considering the important production and loss processes for $O_2(a^1\Delta_g)$ in the E-mode and H-mode of plasma. In both modes production of $O_2(a^1\Delta_g)$ is dominated by electron impact excitation from $O_2(X^3\Sigma_g^-)$ while the most important loss process in the E-mode is deactivation at the chamber walls (loss processes involving reaction with electrons are slow under these conditions due to the low electron densities). As power is increased in the E-mode the increasing electron density leads to increased $O_2(a^1\Delta_g)$ production while the rate of destruction at the walls is approximately constant, this explains the rapid increase in $O_2(a^1\Delta_g)$ density in this mode of operation as power increases.

In the H-mode the opposite trend is observed. The much higher electron densities in this mode mean that electron impact excitation (predominantly to $O_2(b^1\Sigma_g^+)$), electron impact dissociation and electron impact de-excitation become

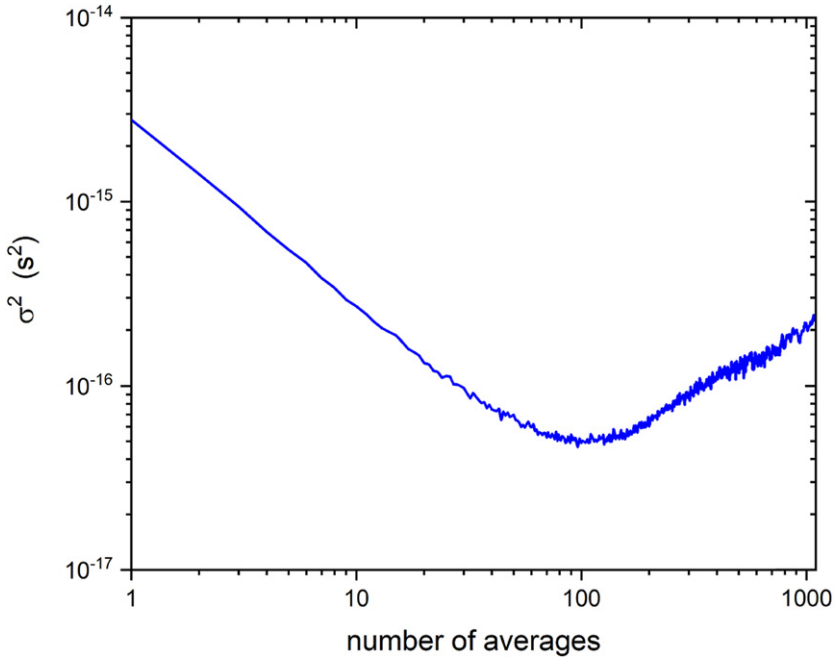

Figure 5. An Allan variance plot to find the minimum detectable amount of $O_2(a^1\Delta_g, v = 0)$ with the laser tuned to the $Q(4)$ line. α_{min} was found to be 1.3×10^{-10} cm^{-1}.

the most important loss processes for $O_2(a^1\Delta_g)$. The involvement of electrons in both production and destruction of $O_2(a^1\Delta_g)$ in the H-mode means that changing electron density has little influence on the equilibrium $O_2(a^1\Delta_g)$ density. Increasing electron temperature (T_e) can influence the balance of loss and production processes (the higher thresholds for the loss processes means that their rates increase more rapidly with increasing T_e) but given that the increase in T_e within the H-mode is expected to be modest, this does not fully explain the reduction in $O_2(a^1\Delta_g)$ density we observe. Rather a potentially important contribution to the observed decrease in $O_2(a^1\Delta_g)$ density with power in the H-mode is gas heating which can be significant in the centre of the chamber (an effect that is masked by the line-of-sight averaged nature of CRDS measurements). This heating corresponds (by the ideal gas law) to a reduced density of $O_2(X^3\Sigma_g^-)$, the precursor to $O_2(a^1\Delta_g)$. The reduction in precursor density is further compounded by the increasing dissociation fraction as power increases leading to slower $O_2(a^1\Delta_g)$ production and a corresponding reduction in equilibrium number density. Meichsner and Wegner [40] report similar changes in the $O_2(a^1\Delta_g)$ number density with power at 38 and 75 mTorr. Quantitative understanding and modelling of the $O_2(a^1\Delta_g)$ density will however benefit from measurements of the absolute density of atomic oxygen over the operating range of the reactor in order to quantify $O(^3P)$ quenching rates in the plasma (a potentially important loss process for excited molecular states [41]), and the levels of vibrational population among the predominant O_2 electronic states (V–T energy transfer with $O(^3P)$ is a crucial process in determining the population of vibrational levels of oxygen molecules in an ICP [42]).

The maximum absorption coefficient measured is ca 6×10^{-9} cm^{-1} (see figure 1) and measurements with high signal-to-noise require an optimised CRD system. The performance of the system can be quantified by the well-known Allan variance [42]. In such an analysis, a series of M measurements of some quantity (say) $y(t)$, where t is the time of the measurement, is made and the data set split into n segments of length Γ; $\bar{y}_k$ is the average value of y in the kth segment. The Allan variance is then:

$$\sigma_y^2(\Gamma) = \frac{\sum_{k=1}^{P_0} \left[\bar{y}_{k+1}(\Gamma) - \bar{y}_k(\Gamma)\right]^2}{2P_0}, \qquad (6)$$

where P_0 is the number of groups or bins that the data set is distributed over. $\sigma_y(\Gamma)$ is recorded for different values of Γ, the averaging time, or n, the number of measurements averaged. Γ and n are related by $\Gamma = n\Gamma_0$, where Γ_0 is the minimum time interval between bins. $\sigma_y^2(\Gamma)$ is then plotted on a log–log plot to find the value of Γ or n needed to minimise the Allan variance. To find the detection limits for this experiment, the ringdown times were recorded over several thousand events and $\sigma_y^2(\Gamma)$ calculated. This was done with the laser tuned to the maxima of the $Q(4)$ and $Q(6)$ lines, and exemplar data for the former case is shown in figure 5. The number of ringdown events that must be averaged for minimum variance is ~100 and corresponds to a minimum detectable absorption coefficient, $\alpha_{min,}$ of 1.3×10^{-10} cm^{-1}. Using the integrated cross section derived for the $Q(12)$ line at 346 K, $\sigma_{int,v=0} = 1.6 \times 10^{-24}$ cm^2 cm^{-1} (from $\sigma_{int,J''} = 2.3 \times 10^{-23}$ cm^2 cm^{-1} and equation (5), realising that $\sigma_{int,v=0}/\sigma_{int,J''} = N_{J''}/N_{v=0}$), yields a minimum detectable line of sight average number density of $O_2(a^1\Delta_g, v = 0)$ of 1.1×10^{12} cm^{-3}.

3. Summary

$O_2(a^1\Delta_g, v = 0)$ has been detected spectroscopically via the (0, 0) vibrational band of the $O_2(b^1\Sigma_g^+) \leftarrow O_2(a^1\Delta_g)$ transition in a low pressure (0.1 Torr) radio frequency pure oxygen ICP. An $O_2(a^1\Delta_g, v = 0)$ concentration of $(9.5 \pm 1.3) \times 10^{13}$cm^{-3} was measured with a detection limit of $\sim 10^{12}$ molecules cm^{-3}, an order of magnitude better than previously reported in the literature [17, 19]. At 300 W power and 100 mTorr pressure the total proportion of the gas that is $O_2(a^1\Delta_g)$ is likely to be ca 5%; as a qualitative comparison, this is significantly lower than, for example, the 12% reported in the case of O_2/He mixtures [43], but similar to VUV absorption measurements in pure oxygen (4%) [16]. The translational and rotational temperatures measured for $O_2(a^1\Delta_g)$ are equilibrated and in good agreement with the translational temperature previously measured for $O(^3P)$ in the same chamber [22]. However, we note that care should be taken interpreting these line-of-sight temperatures, lest they are overly influenced by spatial inhomogeneity. This could occur for example, by a preference for $O_2(a^1\Delta_g)$ to be disproportionately located in cooler areas of the discharge (i.e. close to the walls), and where there are gas number density variations that can lead to the apparent gas temperature as deduced from the measurements being lower than in the plasma bulk. The variation in $O_2(a^1\Delta_g)$ number density with operating power and the lifetime of this state when the plasma is switched off have also been successfully studied. In the former case the $O_2(a^1\Delta_g)$ number density clearly increases as the reactor transitions between E to H modes of operation but subsequently falls at the highest powers where the rates of electron-induced destruction of $O_2(a^1\Delta_g)$ and the effects of gas heating become increasingly significant. The apparent pressure dependence of the wall loss coefficient, similar to that observed for $O(^3P)$ in this chamber, would seem to imply that the ion-bombardment process hypothesised to enhance atomic recombination, by providing more adsorption sites [44], may well also lead to an augmentation of the deactivation of $O_2(a^1\Delta_g)$. The mechanism of this augmentation is uncertain and warrants further investigation. It may involve destruction of the surface oxide layer by ion-bombardment. This would alter the surface-molecule interaction potential and could make electronic energy transfer from the molecule to the metal more facile.

Acknowledgments

The authors would like to acknowledge the UK Engineering and Physical Sciences Research Council (EPSRC) for support provided within the standard research scheme (Grant No. EP/P026621/1) and Lam Research Corporation (US) for a gift award. SDAR would like to thank the Clarendon fund for the award of a graduate scholarship.

Data availability statement

The data that support the findings of this study are available upon reasonable request from the authors.

ORCID iDs

Samuel D A Rogers https://orcid.org/0000-0002-5276-0920
Amelia Bond https://orcid.org/0000-0002-9539-6698
Robert Peverall https://orcid.org/0000-0003-2326-2495
Gus Hancock https://orcid.org/0000-0003-1166-4104
Grant A D Ritchie https://orcid.org/0000-0003-1663-7770

References

[1] Carl D A, Hess D W and Lieberman M A 1990 *J. Vac. Sci. Technol.* A **8** 2924–30
[2] Kitajima M, Kuroki H, Shinno H and Nakamura K G 1992 *Solid State Commun.* **83** 385–8
[3] Ono T, Akagi T and Ichiki T 2009 *J. Appl. Phys.* **105** 013314
[4] Yoshino K, Matsumoto H, Iwasaki T, Kinoshita S, Noda K and Iwamori S 2013 *Vacuum* **93** 84–9
[5] Lee C, Graves D B, Lieberman M A and Hess D W 1994 *J. Electrochem. Soc.* **141** 1546–55
[6] Kiehlbauch M W and Graves D B 2003 *J. Vac. Sci. Technol.* A **21** 660–70
[7] Gudmundsson J T 2004 *J. Phys. D: Appl. Phys.* **37** 2073–81
[8] Gudmundsson J T, Kouznetsov I G, Patel K K and Lieberman M A 2001 *J. Phys. D: Appl. Phys.* **34** 1100–9
[9] Gudmundsson J T and Thorsteinsson E G 2007 *Plasma Sources Sci. Technol.* **16** 399–412
[10] Gudmundsson J T, Kawamura E and Lieberman M A 2013 *Plasma Sources Sci. Technol.* **22** 035011
[11] Toneli D A, Pessoa R S, Roberto M and Gudmundsson J T 2015 *J. Phys. D: Appl. Phys.* **48** 325202
[12] Miller H C, McCord J E, Choy J and Hager G D 2001 *J. Quant. Spectrosc. Radiat. Transfer* **69** 305–25
[13] Findlay F D and Snelling D R 1971 *J. Chem. Phys.* **55** 545–51
[14] Klopovskiy K S, Lopaev D V, Popov N A, Rakhimov A T and Rakhimova T V 1999 *J. Phys. D: Appl. Phys.* **32** 3004–12
[15] Slanger T G and Copeland R A 2003 *Chem. Rev.* **103** 4731–66
[16] Wegner T, Küllig C and Meichsner J 2017 *Plasma Sources Sci. Technol.* **26** 025006
[17] Földes T, Čermák P, Macko M, Veis P and Macko P 2009 *Chem. Phys. Lett.* **467** 233–6
[18] Pazyuk V S, Podmar'kov Y P, Raspopov N A, Frolov M P and Frolov M P 2001 *Quantum Electron.* **31** 363
[19] Gupta M, Owano T, Baer D S, O'Keefe A and Williams S 2004 *Chem. Phys. Lett.* **400** 42
[20] Williams S, Popovic S and Gupta M 2009 *Plasma Sources Sci. Technol.* **18** 035014
[21] Bakowski B, Hancock G, Peverall R, Ritchie G A D and Thornton L J 2004 *J. Phys. D: Appl. Phys.* **37** 2064–72
[22] Peverall R, Rogers S D A and Ritchie G A D 2020 *Plasma Sources Sci. Technol.* **29** 045004
[23] Romanini D, Kachanov A A, Sadeghi N and Stoeckel F 1997 *Chem. Phys. Lett.* **264** 316–22

[24] Vagin N P, Ionin A A, Kochetov I V, Napartovich A P, Podmar'kov Y P, Frolov M P and Yuryshev N N 2005 *Quantum Electron.* **35** 378
[25] Larsson M 1983 *Astron. Astrophys.* **128** 291
[26] Kovács I 1969 *Rotational Structure in the Spectra of Diatomic Molecules* (Bristol: Hilger)
[27] Chiu Y N 1965 *J. Chem. Phys.* **42** 2671
[28] Whiting E E, Schadee A, Tatum J B, Hougen J T and Nicholls R W 1980 *J. Mol. Spectrosc.* **80** 249
[29] Whiting E E, Paterson J A, Kovács I and Nicholls R W 1973 *J. Mol. Spectrosc.* **47** 84
[30] Western C M 2017 *J. Quant. Spectrosc. Radiat. Transfer* **186** 221
[31] Western C M 2018 PGOPHERversion 10.1 (University of Bristol Research Data Repository) https://doi.org/10.5523/bris.3mqfb4glgkr8a2rev7f73t300c
[32] Western C M 2018 Transition matrix elements and line strengths http://pgopher.chm.bris.ac.uk/Help/linestrengths.htm (accessed 29 June 2020)
[33] Demtröder W 2014 *Laser Spectroscopy 1: Basic Principles* 5th edn (Berlin: Springer) p 54
[34] Chantry P J 1987 *J. Appl. Phys.* **62** 1141–8
[35] Winn E B 1950 *Phys. Rev.* **80** 1024–7
[36] Derzsi A, Lafleur T, Booth J-P, Korolov I and Donkó Z 2016 *Plasma Sources Sci. Technol.* **25** 015004
[37] Sharpless R L and Slanger T G 1989 *J. Chem. Phys.* **91** 7947–50
[38] Drouin B J, Gupta H, Yu S, Miller C E and Müller H S P 2012 *J. Chem. Phys.* **137** 024305
[39] Meichsner J and Wegner T 2018 *Eur. Phys. J.* D **72** 85
[40] Volynets A V, Lopaev D V, Rakhimova T V, Proshina O V, Chukalovsky A A and Booth J P 2020 *Plasma Sources Sci. Technol.* **29** 115020
[41] Annušová A, Marinov D, Booth J-P, Sirse N, Da Silva M L, Lopez B and Guerra V 2018 *Plasma Sources Sci. Technol.* **27** 045006
[42] Werle P, Mücke R and Slemr F 1993 *Appl. Phys.* B **57** 131–9
[43] Williams S, Gupta M, Owano T, Baer D S, O'Keefe A, Yarkony D R and Matsika S 2004 *Opt. Lett.* **29** 1066–8
[44] Sarrette J-P, Rouffet B and Ricard A 2006 *Plasma Process. Polym.* **3** 120–6